Microstructure, Tensile Ductility, and Fracture Toughness of Ti-25Al-10Nb-3V-1Mo

C.H. Ward[a], I. Roman[b], J.C. Williams[c], and A.W. Thompson[d]

[a] Wright Laboratory, Wright-Patterson AFB, OH 45433 USA
[b] Hebrew University of Jerusalem, 91904 Jerusalem, Israel
[c] GE Aircraft Engines, Cincinnati, OH 45215 USA
[d] Carnegie Mellon University, Pittsburgh, PA 15213 USA

Abstract

Both the tensile ductility and fracture toughness of titanium aluminide alloys based on Ti_3Al are typically lower than those observed for conventional titanium alloys at room temperature. Six different microstructures were produced to evaluate their effects on these two properties. The microstructures were manipulated through thermomechanical processing to achieve various primary α_2 volume fractions and secondary α_2 morphologies. Room temperature tensile and fracture toughness tests were performed. These were monitored for acoustic emission during mechanical testing to aide in the understanding of the deformation and failure mechanisms. Additionally, flat, pre-polished tensile bars were tested and examined to determine the deformation behavior of the microstructures. This information, together with examination of sectioned round tensile bars, helped identify the microstructural components most critical to failure initiation. The correlation of crack nucleation and propagation to observed properties and microstructure is discussed.

Introduction

The room temperature ductility and fracture toughness of α_2 titanium aluminides have been shown to be dependent on microstructure.[1-8] However, there does not appear to be a significant correlation between these two properties when comparing microstructures. Measurement of acoustic emission (AE) during tensile testing has been used in a recent study to examine the flow and fracture behavior of Ti-25Al-10Nb-3V-1Mo (atomic percent) at room temperature.[9] In that study, it was determined that the events that lead to tensile failure in most microstructures occurred very near the fracture point. Since the nucleation of critical flaws occurs so close to failure, the effect of fracture toughness in extending tensile elongation by delaying crack propagation is negligible. Thus, it must be considered that crack nucleation is the controlling event in the room temperature tensile fracture for most microstructures in α_2 alloys. This study follows the previous report of acoustic emission response during tensile testing and attempts to specifically identify the controlling fracture initiation sites in six different microstructures.

Titanium '92
Science and Technology
Edited by F.H. Froes and I. Caplan
The Minerals, Metals & Materials Society, 1993

Experimental

Six microstructures were prepared by thermomechanical processing (TMP) using hot-die forging and heat treatment. Room temperature tensile tests were performed for each microstructure. Both round and flat geometries were used in tensile testing. The details of the alloy chemistry, TMP, round tensile bar geometries and testing conditions can be found elsewhere.[9] The flat tensile bars had nominal dimensions of 100 mm in length, a 25.4 mm reduced section length, and a 2.75 mm x 9.35 mm reduced cross-section. The flat tensile specimens were polished, with the final polish being accomplished with a colloidal silicate suspended in a basic solution (Beuhler MasterMet). A 12 μm (center to center) square grid (2 μm wide lines) was then applied using the same photo-resist and mask technique used in the production of semiconductors. The grid was etched into the flat tensile bars by the reactive ion technique. Application of the 12 μm grid on the flat tensile bars was generally successful, with a large portion of the gage length containing the pattern. The flat bars were tested in tension at a crosshead speed of 0.02 mm/sec and with a nominal extensometer gage length of 18 mm. Longitudinal cross-sections of the round tensile bars and the surfaces of the flat pre-polished tensile bars were examined using scanning electron microscopy (SEM). Room temperature fracture toughness tests were performed on five of the microstructures according to ASTM E399-89. Compact tension specimens were used having a nominal W=20 mm and B=5 mm. Acoustic emission (AE) response during mechanical testing was monitored for both the round tensile and fracture toughness tests. Specifics regarding the AE monitoring methods have been described in another paper.[9]

Results and Discussion

Tensile Testing

The six microstructures examined in this study are found in Figure 1. A summary of the tensile results are shown in Table I. Significantly lower elongation to failure in the flat tensile specimens is quite noticeable. Failure of at least one of the specimens was caused by a large, apparently machining induced, defect at the surface. The other specimens generally exhibited failure initiation near a specimen corner. This indicates that the sharp corners may have acted as a stress concentrator. Note that the microstructures can be divided into two levels of yield and fracture stress, this is the direct result of of secondary α_2 lath size and morphology.

SEM examination of the flat tensile bars after room temperature tensile testing produced fruitful results. Distortions in the etched grid indicated the scale of deformation on the surface. These distortions can be described in two ways: (1) dislocation slip bands interacting with the grid pattern; (2) the macroscopic effect of slip on causing larger distortions to the pattern.

Table I. Room temperature tensile test results

Microstructure	Type	E (GPa)	YS (MPa)	UTS (MPa)	% Elong.	% ROA	ε_f	σ_f (MPa)
3	Round	94.4	563	806	7.0	9.9	0.104	895
	Flat	100.2	672	NA	NA	6.8		
4	Round	115.1	726	958	6.2	9.4	0.098	1058
	Flat	113.7	745	896	1.6	10.7		
7	Round	104.8	581	821	6.5	8.7	0.091	900
	Flat	104.5	632	725	0.8	9.2		
8	Round	105.9	753	967	5.9	6.7	0.070	1037
	Flat	106.1	711	904	2.1	4.0		
11	Round	90.2	556	745	3.5	6.7	0.069	799
	Flat	88.6	618	656	0.3	1.1		
14	Round	104.0	809	996	3.6	7.6	0.079	1078
	Flat	101.6	727	812	0.6	4.5		

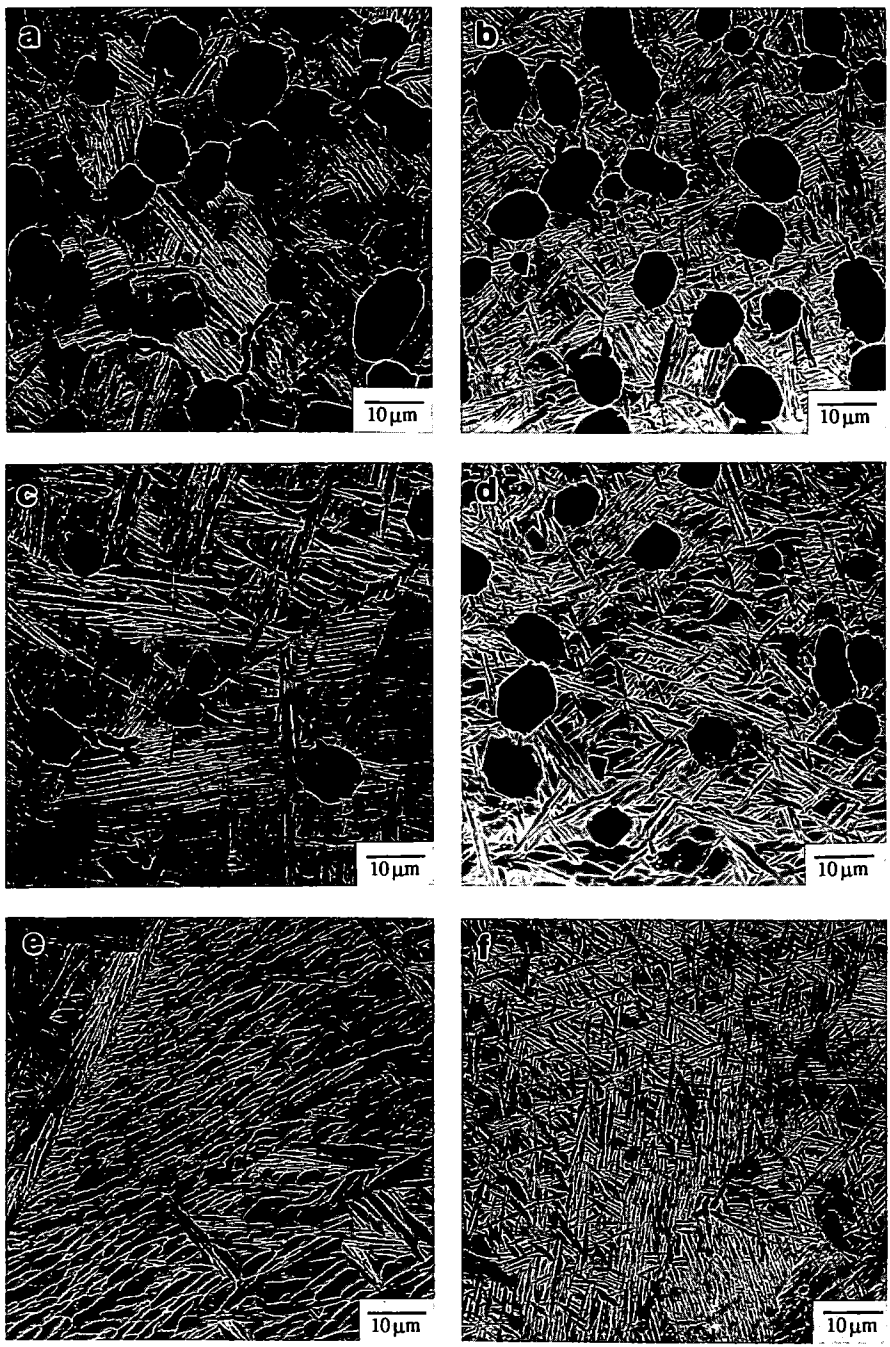

Figure 1 - SEM Micrographs of the microstructures. (a) Forging 3. (b) Forging 4. (c) Forging 7. (d) Forging 8. (e) Forging 11. (f) Forging 14.

The results of AE monitoring of round tensile bars presented previously were identical in behavior between the duplicate tests performed for each microstructure.[9] The output of the transducer was generally quiet from the start of the tensile test, excepting the instances where a yield peak was detected, until very near final failure of the test specimen. Increased acoustic activity was typically observed at strains only within approximately 0.5% of catastrophic failure. This increase in activity is believed to be associated with the nucleation of microcracks in the specimen.

Examination of both the surfaces of the failed flat tensile bars and the cross-sections of the round tensile bars has shown differences in failure initiation sites amongst the different microstructures. Starting with the coarse secondary α_2 lath structure in a β processed material, microstructure 11, slip band intersections on the specimen's surface were profuse with some of these intersections resulting in crack nucleation, Figure 2. Cracks were also observed to occur at the prior β grain boundaries within grain boundary α_2 due to strain incompatibility, Figure 3. This behavior has been previously observed and described by Lukasak and Koss in Ti-24Al-11Nb.[2] Additionally, there was evidence of limited shear crack nucleation.

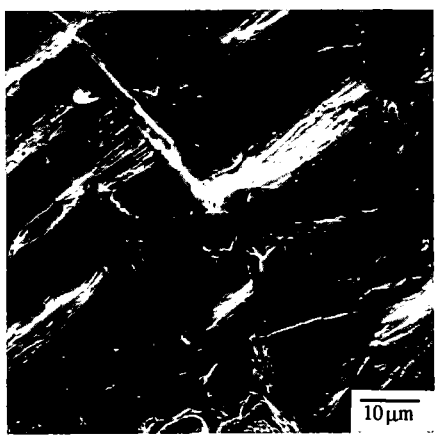

Figure 2 - SEM micrograph of slip band intersections in forging 11.

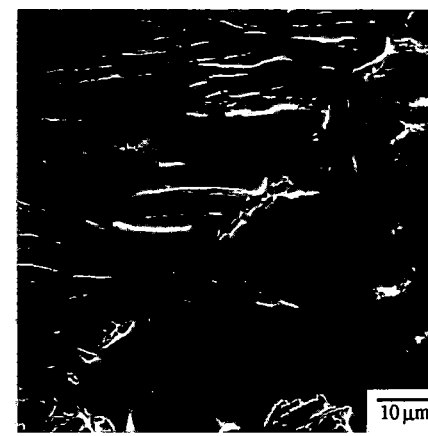

Figure 3 - SEM micrograph of cracking along prior β grain boundary in forging 11.

With the small addition of primary α_2, 0.10 volume fraction, in a coarse microstructure, microstructure 7, some of the cracking observed on the surface of the flat tensile bars was associated with the primary α_2 grains. Slip bands in the matrix were often times seen to have intersected with a failed primary α_2 particle, Figure 4. A large fraction of the cracks observed on the surface were still associated with slip band intersections in the matrix. Increasing the volume fraction of primary α_2 to 0.25 while maintaining a coarse secondary α_2 size, as in microstructure 3, still resulted in long slip bands being a prominent feature on the specimen's surface. However, a larger proportion of cracks were observed to be nucleating at or within primary α_2 grains. The slip band length in microstructures 3 and 7 appeared to be shorter as compared to microstructure 11.

Slip bands were still observed in the β processed microstructure 14, but were on a much finer scale as compared to microstructures 3, 7 and 11. In the fine Widmanstätten microstructure containing 0.25 volume fraction primary α_2, microstructure 4, the initiation sites were almost exclusively associated with the primary α_2 grains. In fact, cracking due to slip band intersections within the fine matrix were not observed. Crack initiation was observed to occur within the individual primary α_2 grains, as in Figure 5, or at the primary α_2/matrix interfaces, as

in Figure 6. The cracks within the primary α_2 grains appeared to be nucleated by two mechanisms. First, as seen in previous studies, some cracks were observed to lie along the operating slip planes and were not oriented perpendicular to the stress axis, Figure 5.[5] The second case found cracks nucleating perpendicular to the stress axis with no apparent slip within the α_2 particles, Figure 7. Thus, the first case appears to be described by shear band decohesion and the second cleavage.

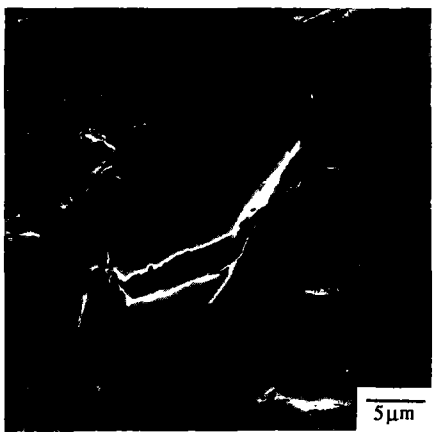

Figure 4 - Matrix slip band intersection with primary α_2 particle in microstructure 7.

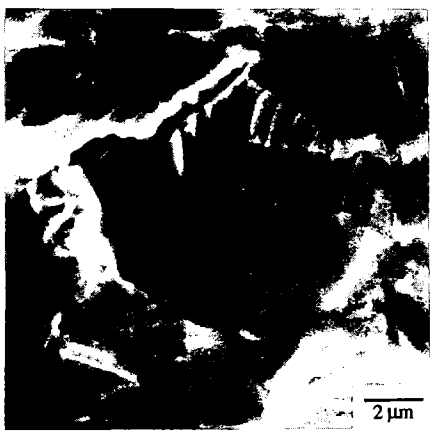

Figure 5 - Failure along active slip planes in a primary α_2 particle in microstructure 4.

Figure 6 - Crack nucleation at the interface of a primary α_2 particle in microstructure 8.

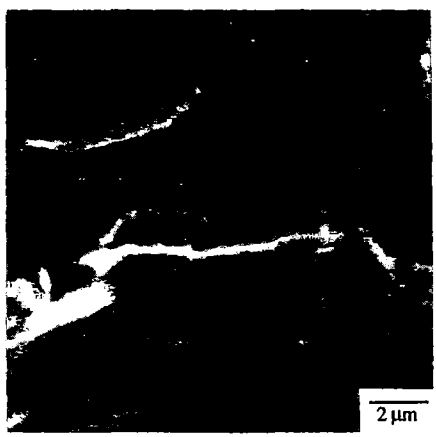

Figure 7 - Cleavage crack nucleated in a primary α_2 particle in microstructure 4.

Longitudinal sectioning of the failed tensile specimens reveals similar crack nucleation sites to those observed on the surface of the pre-polished tensile bars. This result helps validate and generalize the surface observations noted previously. Figure 8 shows crack nucleation at primary α_2/matrix interfaces as well as within primary α_2 particles in microstructure 7. Figure 9 shows crack nucleation associated with grain boundary α_2 and the aligned α_2 laths at prior β grain boundaries in microstructure 11. An enlargement of the crack tip region reveals the

mechanism by which the crack must be propagating, Figure 10. The α_2 laths failed along a plane at an apparent orientation near that of the basal plane. Furthermore, the B2 phase was observed to be pulled up around the α_2 laths as if it had behaved as a plastic bridge or ligament during crack extension.

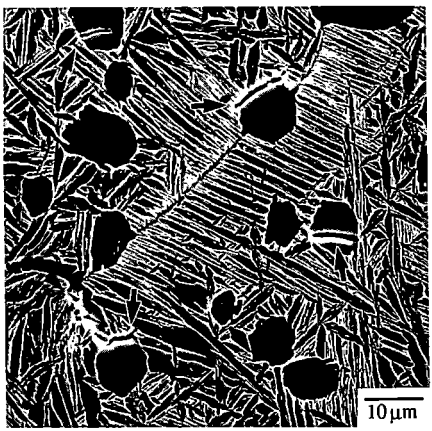

Figure 8 - Sectioned tensile bar showing cracks at interfaces and within primary α_2 particles in microstructure 7.

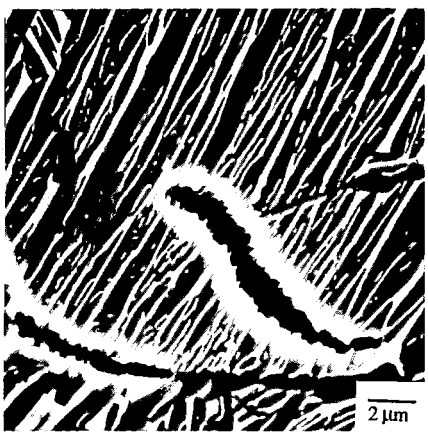

Figure 9 - Cracking associated with prior β grain boundaries in microstructure 11.

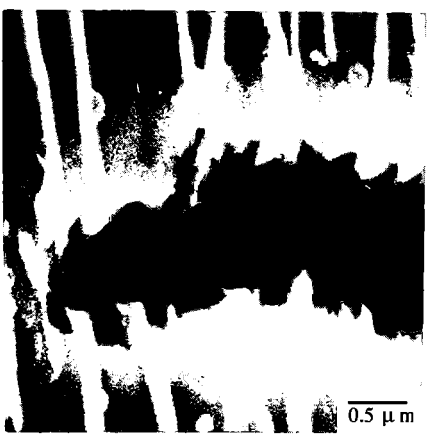

Figure 10 - Enlarged crack tip region of crack in Figure 9.

The behavior of these six microstructures can be grouped into four categories based on stress and strain to failure. Microstructure 11 fails at low stress and strain, whereas microstructure 14 fails at high stress and low strain. Microstructures 3 and 7 fail at low stress but high strain and microstructures 4 and 8 fail at high stress and high strain. Stroh demonstrated that crack nucleation, and hence failure, depends on slip length in brittle fracture.[10] This corresponds to a critical stress at the end of a slip band, which is directly related to the applied tensile stress. As seen above, microstructures 3 and 7 exhibit similar slip band lengths, while those in microstructure 11 are longer, particularly near the prior β grain boundaries. Microstructures 4, 8 and 14, on the other hand, show a much finer slip band length.

Failure in microstructure 11 is dominated by crack nucleation at the prior β grain boundaries. This microstructure has significant amounts of aligned secondary α_2 plates at the prior β grain boundaries which lead to strain incompatibility across the boundaries.[2] The very large effective slip length of these regions due to the alignment of slip planes means rapid strain accumulation at the boundaries and a correspondingly high stress at the end of the resulting slip bands. The high stress at the end of the slip band eventually leads to Stroh crack nucleation at a relatively low applied stress. Rapid propagation of this crack along the prior β grain boundary results in a correspondingly low strain to failure.

Smaller microstructural units of deformation, and thus smaller effective slip lengths, in microstructures 3 and 7 take greater applied stresses than microstructure 11 to nucleate a Stroh crack. These cracks are nucleated at the intersection of a slip band with either another slip band or with a primary α_2 particle. A greater stress to nucleate a crack will obviously result in a larger strain to failure for materials of similar yield stress. Microstructures 4 and 8 having a fine, strong basketweave morphology of secondary α_2 avoid the the formation of slip bands within the matrix and incompatibility across prior β grain boundaries. Thus, an absence of long slip bands intersecting primary α_2 grains means that the applied stress must be even larger to reach a critical cleavage stress. β processed microstructure 14 has a low incidence of aligned secondary α_2 plates at the prior β grain boundary and has a fine, basketweave matrix morphology. It is evident from the tensile data that it started out with a higher yield strength and failed at a similar fracture stress as microstructures 4 and 8, as would be expected for microstructures of similar scale.

As is evident in the micrographs in Figure 1, primary α_2 grains can lie relatively close to one another and have a good probability of being oriented similarly to the tensile axis within a single prior β grain. When one primary α_2 grain fails, the local stress field surrounding this particle is very likely to cause the almost immediate failure of a nearby particle. Thus, it is not surprising that a critical crack size for failure can be reached rapidly by this process. Based on Chan's model of tensile fracture in a brittle material, the low fracture toughness of this material at room temperature is not able contain a moderately sized crack from propagating once one is nucleated.[11] Therefore, tensile fracture occurs very shortly after crack nucleation.

Fracture Toughness Testing

Room temperature fracture toughness tests were performed on all but microstructure 14. The results of testing showed that all five microstructures had a fracture toughness of approximately 20 MPa$\sqrt{m}$, ± 1 MPa$\sqrt{m}$. The first thing to note is that these are amongst the highest fracture toughness values reported for Ti-25-10-3-1, which are typically closer to 15 MPa$\sqrt{m}$.[12,13] No significant trends were observed in the fracture toughness results. Most fracture surfaces were observed to exhibit very flat fracture surfaces, although that of microstructure 11 had a visually more tortuous appearance. The coarse aligned microstructure of microstructure 11 would have been expected to have a higher fracture toughness value than the other microstructures based on results obtained by Marquardt.[6] However, while the coarse secondary α_2 laths are aligned in regions, this microstructure cannot be termed 'colony', as was the case in Marquardt's study. Additionally, the prior β grain size in this microstructure is found to be smaller than for all other microstructures, 0.6 mm *vs.* 1 mm. This is due to the one hour β anneal after forging; evidently the time allowed for solution treatment was insufficient to permit substantial β grain growth after recrystallization. No significant differences in AE response amongst the six microstructures were found during fracture toughness testing.

Summary and Conclusions

The behavior of these microstructures at room temperature was studied by monitoring the acoustic emission response during mechanical testing. Failure was generally found to be preceded by very little acoustic emission activity, indicating failure primarily controlled by the crack nucleation event. The length of slip bands formed in the secondary α_2+B2 matrix during

plastic deformation was found to control the fracture stress of these microstructures. SEM examination showed the differences in crack nucleation sites within the six microstructures. Failure initiation ranged from crack nucleation at slip band intersections and shear cracking in coarse β processed microstructure, to cleavage, slip band decohesion and interfacial failure associated with primary α_2 grains in $\alpha_2+\beta$ processed microstructures. A β processed microstructure with a coarse microstructure exhibited lower ductility due to the presence of aligned secondary α_2 laths at prior β grain boundaries, leading to strain incompatibility across the boundaries at a low applied stress. Coarse $\alpha_2+\beta$ processed microstructures were found to have nucleation sites associated with both slip band intersections in the matrix and slip band intersections with primary α_2 particles. Conversely, fine $\alpha_2+\beta$ processed microstructures appear to nucleate failure solely at primary α_2 particles. A β processed microstructure with a fine microstructure failed at a lower strain but a similar fracture stress as in the fine $\alpha_2+\beta$ processed microstructures. Thus, failure does appear to be controlled by a critical cleavage stress which is determined by the microstructural unit controlling slip band formation.

Although the fracture toughness values reported for the material in this study are relatively high for this alloy, ~20MPa$\sqrt{m}$, no significant effect of microstructure on toughness was observed. It should also be noted that the strength levels reported in this study are lower than those previously reported for this alloy, and likewise the ductility is higher than seen before. Thus, the relatively subtle effect that microstructure has been shown to have on the fracture toughness of these alloys may be masked by an increased capacity for plastic work in the present material.[5,7,8]

Acknowledgements

The authors greatly appreciate the experimental assistance received from J. Eblin, J. Ruschau and J. Eschweiler. One author (CHW) would like to thank Dr. M. Peters for providing the facilities of the German Aerospace Research Establishment (DLR) where part of this work was completed.

References

1. C.H. Ward, J.C. Williams, A.W. Thompson, D.G. Rosenthal, and F.H. Froes, Sixth World Conference on Titanium, ed. P. Lacombe *et al.*, (Les Ulis Cedex, France: les éditions de phisique, 1989), 1103.

2. D.A. Lukasak and D.A. Koss, Met. Trans., 21A (1990), 135.

3. J. Kumpfert, K.-J. Grundhoff, H. Schurmann, Y.T. Lee, C.H. Ward, and M. Peters, Proc. Conf. 'Euromat '91', (London: The Institute for Metals, in press).

4. C.H. Ward and S.J. Balsone, Microstructure/Property Relationships in Titanium Aluminides and Alloys, ed. Y-W. Kim and R.R. Boyer, (Warrendale, PA: TMS, 1991), 373.

5. K.S. Chan, Met. Trans., 21A (1990), 2687.

6. B.J. Marquardt, "Fracture Toughness of Alpha-2 Titanium Aluminides" (Paper presented at AeroMat '90, Long Beach, CA, 23 May 1990).

7. K.S. Chan, Met. Trans., 23A (1992), 183.

8. W.O. Soboyejo, Met. Trans., 23A (1992), 1737.

9. I. Roman and C.H. Ward, Scripta Met., 24 (1992).

10. A.N. Stroh, Adv. Phys., 6 (1957), 418.

11. Kwai S. Chan, Scripta Met., 24 (1990), 1725.

12. M.J. Blackburn and M.P. Smith: "R&D on Composition and Processing of Titanium Aluminide Alloys for Turbine Engines," AFWAL Technical Report 82-4086, Wright-Patterson AFB, 1982.

13. D.P. DeLuca and B.A. Cowles, "Fatigue and Fracture of Titanium Aluminides," WRDC Technical Report 90-4075, Wright-Patterson AFB, 1990.